

In-situ Laser synthesis of rare earth aluminate coatings in the system Ln -Al-O ($Ln=Y, Gd$)

I. de Francisco¹, V. V. Lennikov¹, J.A. Bea², A. Vegas^{3*}, J. B. Carda⁴ and G. F. de la Fuente^{1*}

¹Instituto de Ciencia de Materiales de Aragón (CSIC-Univ. Zaragoza), E-50018 Zaragoza, Spain

²Group of Structural Mechanics and Material Modeling, Aragón Institute of Engineering Research (I3A), University of Zaragoza, Spain

³ Instituto de Química-Física Rocasolano, CSIC, Serrano 119, E-28006 Madrid, Spain

⁴Dept. Química Inorgànica i Orgànica, Universitat Jaume I, E-12071, Castellón de la Plana, Spain

Abstract

Laser Zone Melting (LZM) was employed in this work to prepare Ln -Al-O coatings on polycrystalline Al_2O_3 substrates, using the corresponding mixtures of powdered rare-earth oxides and Al_2O_3 as starting materials. In-situ synthesis of the compounds $Ln = Y, Gd$ was performed using a CO_2 laser, emitting at 10.6 μm . Microstructure (SEM) and phase nature (XRD) demonstrated in-situ formation of $Al_2O_3/Y_3Al_5O_{12}$ (YAG) and $Al_2O_3/GdAlO_3$ (GAP) eutectic systems. The interaction with the substrate resulted in mechanically stable, well integrated 200-500 μm thick composite coatings, as observed in nanoindentation tests. The phase relations found in these materials are consistent with the crystallographic concepts advanced by Vegas (Ramos-Gallardo & Vegas, J. Solid State Chem. 128 (1997) 69), where cation sub-arrays are proposed to play an important role in governing metal oxide structures. These sub-arrays are suggested as the structural drive behind eutectic oxide formation. LZM proves to be a convenient method to investigate the behaviour of complex oxide systems at high temperature, to apply a rational concept towards the understanding of phase relations and to develop design criteria for oxide coatings.

Keywords: Laser Zone Melting, eutectic, $Y_3Al_5O_{12}$ coating, $GdAlO_2$ coating, Al_2O_3 , aluminates

*Authors to whom correspondence may be addressed.

|

1. Introduction

In the last 20 years several [papers](#) have outlined the key importance of the cation sub-arrays in inorganic oxides [\[1-5\]](#), governing their crystal structures, as well as offering a rational explanation for them. One of the most important issues derived from those studies is that, in many oxides, their cation sub-arrays have identical structure as the parent alloy. O’Keeffe & Hyde [6] reported the first examples of such odd features which were seen as singular coincidences. Further structural analyses carried out by Vegas and co-workers [1-4] proved these structural similarities to be more universal than believed. As illustrating examples, it is worth mentioning how the structure of the [BaSn alloy \(CsCl-type\)](#) high pressure phase is preserved in the [BaSnO₃](#) perovskite [3]. The same occurs with the *LnAl* alloys (also CsCl-type) and their corresponding *LnAlO₃* perovskites [4]. The most remarkable feature is, however, that in all these cases, the unit cell dimensions of the alloy remain unaltered, in spite of the insertion of the O atoms [3-4].

The cubic Laves-Friauf phases (MgCu₂-type) and spinels like MgAl₂O₄ provide another example of such structural coincidences, since the MgAl₂ sub-array in spinel is isostructural with MgCu₂. The interest is even greater because the *LnAl₂* alloys, strongly related to *LnAl*, are also MgCu₂-type.

It should be remarked that formal *Ln³⁺* and *Al³⁺* cations do not satisfy the valence requirements to form the [LnAl₂O₄](#) spinels. However, the valence rules are obeyed in the [Ln₃Al₅O₁₂](#) garnets. These two families of compounds, apparently unrelated, can have much in common if we think that a hypothetical [LnAl₂O₄](#) spinel (written as Ln₃Al₆O₁₂), might formally be converted into the *Ln₃Al₅O₁₂* [garnet](#) by only removing 1/6 of the Al

atoms. This leads us to think that the alloys in the *Ln/Al* system are also intimately related to the cation arrays of their oxides as deduced from the works of Vegas [and co-workers](#) [1-4].

A consequence of this concept leads to the question of whether the cation arrays would also be the subjacent principle controlling eutectic phase formation. If that [was](#) the case, it would suggest that some [kinds](#) of chemical and structural [similarities](#) must occur between the cation sub-arrays in the two phases forming a eutectic.

Aluminate coatings are very interesting [to improve](#) the surface properties of materials like alumina, porcelain, as well as a diversity of refractory and clay tiles. Composites [consisting](#) of a ceramics matrix embedded with strong ceramic fibers, are known to exhibit improved toughness and strength, because their brittleness is reduced by the fiber/matrix interface. Recently, unidirectional solidification methods were applied to produce $\text{Al}_2\text{O}_3\text{-Y}_3\text{Al}_5\text{O}_{12}$ (YAG) [7] and $\text{Al}_2\text{O}_3\text{-GdAlO}_3$ [8] eutectic ceramic composites. The unidirectionally solidified $\text{Al}_2\text{O}_3\text{-YAG}$ eutectic composite exhibited high strength, thermal stability and creep resistance at high temperatures [8-11]. $\text{Al}_2\text{O}_3/\text{GdAlO}_3$ eutectic composites have also been produced by unidirectional solidification, providing [an](#) eutectic composite with high strength and resistance to brittle failure even at high temperatures [8].

The important advantage of aluminates is their potential chemical compatibility with alumina and porcelain-like ceramic materials. The fact that they contain aluminium oxide components opens the possibility to obtain coatings with good interface strength and satisfactory chemical purity.

The recently developed “in-situ” synthesis laser zone melting method [12-14], which makes use of a CO_2 laser scanner combined with simultaneous external heating of the substrate and its uniform movement [14, 15], allows to obtain coatings of practically

any oxide material on the alumina substrate. This is particularly advantageous if the coating material is chemically compatible with aluminium oxide and if the phases obtained during melting exhibit intrinsically high boiling temperatures. The method may be applied to produce a wide spectrum of materials and it enables the investigation of phase relations, after solidification from the melt, for oxide systems with extremely high melting points (up to 3000°C). These may conform a difficult to access zone within the Energy Landscape of solids described in Jansen's Synthesis Planning pioneering work [16].

The objective of the present work is to develop a novel protocol of coating design using the Vegas concept. In addition, the latter will be applied to explore phase relations within the coatings obtained by laser zone melting.

2. Experimental

2.1. Precursor preparation

Precursors were prepared from the following compositions: Y_1 with the stoichiometric composition of perovskite-type yttrium aluminate and Y_2 with the stoichiometric composition of yttrium aluminium garnet. In the case of gadolinium compositions, G_1 represents the stoichiometric composition of perovskite-type gadolinium aluminate and G_2 the stoichiometric composition of gadolinium aluminium garnet (Table I).

Precursor coatings were obtained from the pure oxides Al_2O_3 (SIGMA-ALDRICH, 99.7%), Gd_2O_3 (ALFA-AESAR, 99.9%) and Y_2O_3 (99.99%). The starting powder materials were milled in a Retsch 2000 Ball Mill (model MM2000, Resch, Haan, Germany) using alumina components, with isopropyl alcohol (PANREAC, chemical purity) as a liquid suspension medium with a solid content ranging between 68 and 74% in weight. The resultant suspension was deposited onto commercial $8 \times 10 \times 1 \text{ mm}^3$

polycrystalline (mean grain size ca. 3 μm) alumina plates using the dip-coating method.

The substrate was immersed into the suspension and extracted vertically at a speed of 10 mm s^{-1} . The coated plates were dried for a period of 48 h at room temperature before laser processing.

2.2. Laser Zone Melting (LZM)

The LZM process was performed using a Rofin-Sinar 350W SLAB-type CO_2 laser emitting at a wavelength $\lambda = 10.6 \mu\text{m}$. The laser beam was directed through an optical beam steering system, which transformed the circular cross-section beam into a line measuring 1 mm in thickness and a variable width. In all samples the width was set at 40 mm.

The line was directed to the sample at a normal angle with the orientation shown in Fig. 1, where the LZM device is illustrated. The stage movement speed was established at 1500 and 3000 mm h^{-1} . The laser power was fixed at 350W for all of the sample treatments. In order to avoid cracks, the samples were simultaneously externally heated with a resistance furnace in a temperature range between 700 and 1200 $^\circ\text{C}$.

2.3. Characterisation

The crystalline phases of the samples were studied by X-Ray diffraction using a D-Max Rigaku diffractometer ($\text{CuK}\alpha$) with a rotating anode. The microstructure of sample surfaces, as well as their polished longitudinal and transversal cross-sections (with respect to the treatment direction) were studied using a JEOL 6400 scanning electron microscope. Elemental analyses were performed during SEM observation using a coupled Oxford Instruments EDS unit.

Nanoindentation tests were conducted with a Nano Indenter G200 (Agilent Technologies, Inc.). Tests were performed on polished sample longitudinal cross-sections (with respect to the solidification direction). An array of 100 indentations was performed in each sample studied within a 25x4 matrix with 20 μm spacing between indentations. Each indentation array was started at surface of the coating and ended deep into the substrate, in order to study the mechanical behaviour of the samples along their cross section and identify potential Heat Affected Zones (HAZ) or the effect of changes in microstructure or phase composition. The tests were performed with a constant drift rate of 0.05 s^{-1} and a depth limit of 2000 nm, using the trigonal Berkovich indenter and fused silica for standard area-function calibration.

3. Results and discussion

3.1. XRD Characterisation

According to X-ray diffraction measurements obtained on the surfaces of the laser-prepared samples, important differences are observed in the crystalline phases found as a function of the rare earth element present. The main interest aroused from the concurrent formation of two types of phases: the perovskite (LnAlO_3) and the garnet ($\text{Ln}_3\text{Al}_5\text{O}_{12}$). At a first glance, the formation of the garnet should have occurred when the Al_2O_3 rich composition (Y_2) was used, as in the other composition (Y_1) there was not sufficient alumina content in the precursor to reach the equilibrium state. This may be true in case of using the traditional ceramic synthesis with diffusion processes dominating the associated solid state reactions: the substrate material should react to a limited extent and not play an important role in phase formation. In the present work, the reaction zone is melted and the substrate starts to play a relevant role in the process.

The alumina substrate was selected in order to limit the number of possible reactions which would lead to an undesired final phase composition. Thus in the molten zone formed there is an excess of aluminium oxide, as confirmed by diffraction patterns obtained on Y-containing samples (Fig. 2a, b). In spite of the precursor composition used in sample Y₁, the formation of the Y₃Al₅O₁₂ garnet phase occurs. As observed in these figures, the pattern of Al₂O₃ is present in both samples, but its peaks are shifted by ca. 0.5 theta degrees. This is due to the main signal of aluminium oxide that comes from the substrate, about 200 to 450 μm lower than the molten layer. The peaks corresponding to Y₂O₃ were not found in the sample with nominal composition YAIO₃, consistent with the participation of the substrate in phase formation of the final product, and probably because it was below the detection limit of the XRD system employed.

The phase relations in this particular system depend not only on the chemical composition of the starting mixture. The thermodynamic stability of the products of the reaction may be largely controlled by the available crystal structures within this system.

In addition, kinetics may provoke the formation of unusual phases within the frame of the LZM method, since rapid directional solidification is applied to the molten oxide mixture.

One of the objectives of this work is to clarify whether the conditions of the laser melt synthesis are near the equilibrium state at the temperature given, or if the kinetic factors play a dominant role in phase development. This is key knowledge to apply laser melting to the investigation of high melting oxide systems. If the phases detected correlate with those that will be formed in accordance with the cation sub-array crystallographic concept [1-4] and found on conventional phase diagrams [17-19], then the conditions here imposed are likely near the thermodynamic equilibrium. The kinetic behaviour of the system should thus only affect the microstructure of the sample, the

crystallite size and distribution, but not the final phase composition. This statement may be applied to our objectives if the products are $Y_3Al_5O_{12}$ and $GdAlO_3$, respectively.

The X-ray diffraction [diagrams](#) of samples with gadolinium content are presented in Fig. 3. In spite of the processes resulting in excess of Al_2O_3 in the reaction zone, only the peaks corresponding to the $GdAlO_3$ perovskite are present in the diffraction pattern. As in the previous Y system, the slightly shifted pattern of Al_2O_3 is also found.

The XRD analysis thus suggests that for all the Y- and Gd-containing samples the process is controlled thermodynamically, resulting in the phases reported for the systems studied. It is thus possible to use this laser melting method to investigate the oxide systems at high temperatures near equilibrium conditions, where conventional furnaces cannot melt these materials.

It should be mentioned that the XRD [analyses](#) evidence that the presented coatings exhibit a certain degree of texture, developed during laser zone melting. This follows from modified peak intensity ratios for the observed reflections, expected for each of the crystalline phases present within each sample. The comparison of the intensity of the peaks of Al_2O_3 suggests that texturing affects not only the outermost surface layer, but also part of substrate, as expected from the directionality and melt depth reached with LZM. The solidification rates, controlled by the sample travelling rates used here, however, are too high to provoke exaggerated texture features on the products obtained, as is the case for eutectic [12] or superconductor [13] oxides obtained previously at low traverse rates.

3.2. SEM observations

CO_2 laser surface treated rare earth aluminate coatings on alumina substrates have been observed by scanning electron microscopy, where the presence of two different eutectic

compositions was revealed. A binary $\text{Al}_2\text{O}_3/\text{Y}_3\text{Al}_5\text{O}_{12}$ (YAG) eutectic coating has been obtained from the starting Y_1 and Y_2 compositions. It consists of cells of an interpenetrating network of two phases, YAG (gray contrast), and $\alpha\text{-Al}_2\text{O}_3$ (black contrast), surrounded by $\alpha\text{-Al}_2\text{O}_3$. The starting G_1 and G_2 compositions generated a coating of $\text{Al}_2\text{O}_3/\text{GdAlO}_3$ (GAP) binary eutectic that consists of cells of an interpenetrating network of GAP (gray contrast area) and $\alpha\text{-Al}_2\text{O}_3$ (black contrast area), surrounded by $\alpha\text{-Al}_2\text{O}_3$. [The microstructure given for each composition can be observed in Fig. 4.](#) The observation of the eutectic zones agrees with former reported microstructures [8, 19].

Due to the Al_2O_3 excess originated by the convective movements within the melt during the laser treatment [12, 14], faceted $\alpha\text{-Al}_2\text{O}_3$ zones have been formed in all compositions. This excess cancels the effect of the Al_2O_3 starting composition on the resultant microstructure observed for the two different samples derived from each rare earth. [although recent experiments have demonstrated that the presence of Alumina as a precursor component does affect its final thickness to some degree. This will be the subject of an upcoming paper.](#)

Table I shows that the starting sample compositions in Y_1 , Y_2 , G_1 and G_2 , are quite different from the eutectic compositions [4, 5]. In all cases, the starting compositions are deficient in Al_2O_3 compared with the eutectic ones. Convection movements during laser treatment have partially melted the alumina substrate, generating an extra contribution to the alumina amount that allows the eutectic growth. This extra alumina also permits the alumina recrystallisation that forms faceted $\alpha\text{-Al}_2\text{O}_3$ zones, as Fig. 4 shows. The recrystallisation appears associated to the high temperatures and thermal stress present at the substrate surface. These induce breakdown of intergranular forces

and cause an important uptake of grains into the melt. Recrystallisation of these grains takes place directionally at the solidification front [12].

Fig. 4 shows that the coatings obtained are free of cracks at the coating-substrate interface. This interface is formed by faceted α -Al₂O₃ zones with the presence of YAG or GAP (according to the composition) in the interstitial space between them, in the proximity of the coating, and a transition zone with grains of unaffected substrate (alumina grains) and YAG or GAP in their interstitial spaces. In this zone, phases from both, substrate and coating, are found to conform a new multiphase adjusting layer in accordance with the downward diffusion of the coating component into the substrate.

Fig. 5 and Table II show the differences in composition across the coating-substrate interface as determined by EDS. The micrograph in Fig. 5 shows the elemental microanalysis areas taken on sample Y₁ across the coating-substrate interface. Analyses were performed in a similar fashion in the rest of the samples. Table II shows the downward diffusion across the interface in terms of the Y and Gd compositions determined. Microanalysis was performed in areas separated approximately by 45 μ m.

The stage movement speeds used to process the samples were 1500 and 3000 mm h⁻¹.

Fig. 6 corresponds to the secondary electron micrograph of samples with a composition type Y₁, obtained at stage movement speeds of 1500 mm h⁻¹ and 3000 mm h⁻¹, respectively. It shows a clear difference between the size of the faceted α -Al₂O₃ zones in the two samples. The sample grown at 1500 mm h⁻¹ shows the α -Al₂O₃ zones larger than the α -Al₂O₃ zones in the sample grown at 3000 mm h⁻¹. At processing rates of 3000 mm h⁻¹, the growth of the alumina phase is limited by higher cooling rates of the melt.

For a given set of laser conditions and a scanning speed fixed at 1500 mm h^{-1} , the thickness of these coatings ranges from 200 to 450 μm . The diffusion zone thicknesses are found similar for compositions with the same rare earth: Y_1 and Y_2 present a diffusion zone of 250 μm , while G_1 and G_2 exhibit a diffusion zone of 300 μm .

3.3. Mechanical properties. Nanoindentation.

Nanoindentation experiments were carried out in order to measure the coating hardness and compare it with the polycrystalline alumina substrate hardness. In [each of the studied samples](#), the coating hardness is found to be very similar to that of the polycrystalline alumina substrate. This includes the transition zone, between the coating and the substrate, as well as the affected substrate to the complete indentation depth.

The average value measured is around 20 GPa, [similar to previous values reported in the literature \[20-21\]](#). The coating hardness values obtained do not appear thus to depend on the particular $\text{Al}_2\text{O}_3/\text{Y}_3\text{Al}_5\text{O}_{12}$ (YAG) or $\text{Al}_2\text{O}_3/\text{GdAlO}_3$ (GAP) eutectic composition. In general, this could be explained by [the high content of alumina found in the eutectics \(Table I\)](#) and the similarity of the crystallographic structure of the second eutectic component, which will be discussed later.

Coatings are formed by cells of the corresponding eutectic compositions ($\text{Al}_2\text{O}_3/\text{Y}_3\text{Al}_5\text{O}_{12}$ (YAG) or $\text{Al}_2\text{O}_3/\text{GdAlO}_3$ (GAP)) and faceted $\alpha\text{-Al}_2\text{O}_3$ zones. Depending on the sample, the size of the faceted $\alpha\text{-Al}_2\text{O}_3$ zones may be greater than the indentation size. Thus, the indentation may take place on a faceted $\alpha\text{-Al}_2\text{O}_3$ zone. In this case, if the eutectic hardness is slightly lower than that of the faceted $\alpha\text{-Al}_2\text{O}_3$, the indenter could drag the faceted $\alpha\text{-Al}_2\text{O}_3$ zone downward and the hardness data would be controlled not by the indenter form but by the form of $\alpha\text{-Al}_2\text{O}_3$. This phenomenon produces some scattering in the obtained data. The graphics presented in Fig. 7. show

that samples treated at 3000 mm h⁻¹ present less scattering than those treated at 1500 mmh⁻¹, consistent with and attributed to the greater size of faceted α -Al₂O₃ zones in the samples solidified at lower rates. Most of the scattering noise is situated between the beginning and the middle zone of the curves, corresponding to the coating-interface-transition zone of the sample. The latter section of the curves correspond to the polycrystalline α -Al₂O₃ substrate zone, where lower scattering is observed. As shown previously, faceted α -Al₂O₃ zones in 1500 mm h⁻¹ samples were larger than those in 3000 mm h⁻¹ samples, consistent with the latter observations.

3.4. Structural Relations and Eutectic phase formation

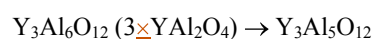
The laser zone melting method applied here to obtain Perovskite and Garnet type aluminate coatings on alumina substrates revealed that the rare-earth element introduced played an important role in the final product obtained. Under the laser synthesis conditions imposed, yttria-containing samples yielded Y₃Al₅O₁₂ garnet, while gadolinia-containing samples yielded GdAlO₃ perovskite. Intense interaction with the substrate induced, in addition, the formation of eutectic microstructures which, for the Al₂O₃-Y₂O₃ system have been previously studied with respect to the relative stability of the perovskite and garnet phases as a function of temperature and cooling rate [22]. In the latter study, thermodynamic stability and nucleation criteria were taken into account in order to justify the type of eutectic product obtained from the melt. In accordance with the previous report, and consistent with the presence of excess Al₂O₃ from the substrate, the composition of the deposited Ln-Al₂O₃ precursor was found here to play a minor role in the final phase obtained. Nevertheless, thermodynamic conditions may not sufficiently justify the preference for specific types of structures within a given system.

An alternative explanation, based on structural considerations, is thus proposed here for the above observations.

Following the concept introduced earlier by Vegas [1-4], the preservation of the corresponding alloy structures in the oxides may offer a rational explanation for the phenomena observed in these experiments. The structural coincidences reported for both, $LnAlO_3$ and $Ln_3Al_5O_{12}$ [2] in which the structural features of various alloys in the Ln -Al system ($LnAl$, Ln_3Al and $LnAl_3$) are preserved, clearly show that the cation skeletons are determinant for both, the structure and eutectic compound product formation as found here.

In support of this assertion, the existence of compounds of formula $LnAl_2$ with the structure of the cubic $MgCu_2$ Laves phases is worthy of mention. Similarly, alumina also forms a γ -phase of formula $Al_{2.8}O_4$ which is considered as an aluminium defect spinel, where the aluminium atoms are also arranged as in the Laves phases. As it was advanced in the introduction, however, the oxidation of the YAl_2 alloy cannot yield a hypothetical spinel of formula YAl_2O_4 . Alternatively, formation of the $Y_3Al_5O_{12}$ garnet can be derived from the segregation of 1/6 of the Al atoms of the spinel structure.

The process can be represented as



Both structures, spinel and garnet, are strongly related, as has been shown for the similar compounds Fe_2SiO_4 and $Fe_5Si_3O_{12}$ [23]. The suggested transformation between both structures is quite plausible because it conforms to the principle of minimal fragmentation and displacement, illustrated in Fig. 8. A fragment of the hypothetical Al_2LnO_4 spinel structure has been represented on the left side of Fig. 8. It consists of the truncated tetrahedron formed by 12 Al atoms centered around the Ln atom. Note, however, that this arrangement is the one forming the real $LnAl_2$ Laves phases and that,

in the MgAl_2O_4 spinel itself, the Al_{12} polyhedron is centered around the Mg atom. The latter is coordinated by four O atoms, forming an MgO_4 tetrahedron.

If we notionally insert the O atoms to form Al_2LnO_4 , the structure should react segregating 1/6 of the Al atoms in order to fit the required stoichiometry. This segregation is illustrated in the central drawing of Fig. 8, where the two fictitious atoms have been inserted in the upper and lower edges of the Al_{12} truncated tetrahedron. These fictitious atoms are in fact one of the two Al atoms forming the edges. When one of these atoms is removed, the remaining atoms migrate towards the centre of the old edges, forming thus a new Al_{10} polyhedron. In this central drawing both the Al_{10} and Al_{12} polyhedra have been illustrated. However, the drawing on the right represents the final Al_{10} polyhedron, which is that existing within the $\text{Ln}_3\text{Al}_5\text{O}_{12}$ garnet. Another relevant issue is that in both structure types, spinel and garnet, the centering atoms (Mg, Ln) form a diamond-like network, a feature that reinforces the similarities between both structures. These similarities also give support to the idea that similar cation arrays in oxides might well be the driving force behind the formation of eutectics.

Thus, the eutectic Al_2O_3 - $\text{Y}_3\text{Al}_5\text{O}_{12}$ can be thought of as the consequence of the similar network formed by the Al atoms in the defective spinel-like γ - Al_2O_3 ($Fd-3m$) and that of $\text{Y}_3\text{Al}_5\text{O}_{12}$ (see Fig. 8). It is noteworthy that in the Al_2O_3 - Y_2O_3 system, the alumina-garnet eutectic is observed under normal conditions, whereas the alumina-perovskite composite has been only observed as a metastable system. In this context, it is worth mentioning that the YAlO_3 perovskite is stable only above 1873 K [24].

In the case of the Al_2O_3 - Gd_2O_3 system, however, the observed eutectic is not Al_2O_3 - $\text{Gd}_3\text{Al}_5\text{O}_{12}$ but rather the alumina-perovskite (Al_2O_3 - GdAlO_3). This contrast in behaviour might be explained starting from the same Laves phase GdAl_2 which, by a gradual increase in Gd content, could give rise to either a metastable b.c.c. (body centred cubic)

structure or disordered CsCl-type structure. This transformation has been reported for the NbCr₂ Laves phase [25], which converts into a metastable b.c.c. phase by mechanical alloying. This last conversion opens the possibility for LnAlO₃ perovskite formation from the LnAl₂ Laves skeleton [26].

The above discussion suggests that there exists a close structural relationship between all the phases known within the Al-Ln system and the cation arrays or sublattices of the known ternary oxides. Starting from the YAl₂ Laves phase, a structural pathway leading to the garnet structure Y₃Al₅O₁₂ is proposed. As mentioned earlier, the intermediate state might well be the non-existing YAl₂O₄ spinel. In the case of the perovskite, a gradual change from Gd₃Al₅O₁₂ to Gd₄Al₄O₁₂ would similarly lead to the final GdAlO₃.

The high pressure and high temperature behaviour of the piroxene MgSiO₃ also supports these arguments: MgSiO₃ undergoes the piroxene → perovskite transition at high pressures [27]. If pressure and temperature are applied simultaneously, the piroxene structure converts into a garnet-like structure in which ¼ of the silicon atoms are mixed with the magnesium atoms, giving rise to the garnet (Mg₄Si)Si₃O₁₂ [28].

3.5. Conclusions

The laser zone melting (LZM) method was applied to obtain coatings on alumina substrates using previously deposited precursors containing Y and Gd and Al oxide mixtures with the perovskite and garnet stoichiometries. Composite perovskite and garnet type eutectic coatings were thus synthesized in-situ, as a function of the rare-earth element introduced. In particular, the yttria-containing samples formed the Y₃Al₅O₁₂ garnet, while the gadolinia-containing samples formed the GdAlO₃

perovskite. Intense interaction with the substrate, induced by the extreme high temperatures reached and by melting, followed by directional solidification, resulted in formation of $\text{Al}_2\text{O}_3/\text{Y}_3\text{Al}_5\text{O}_{12}$ and $\text{Al}_2\text{O}_3/\text{GdAlO}_3$ eutectic microstructures. The composition of the deposited starting precursor played a minor role in the final product phase composition. Nevertheless, mechanically stable, well integrated 200-500 μm thick composite coatings with similar properties to corresponding bulk materials reported in the literature, were obtained as observed by nanoindentation tests.

An alternative view on eutectic formation is proposed in this work based on the importance of cation-sublattices, found as the building blocks in oxides and as the structural drive towards eutectic formation. This paper proves that LZM is a convenient method to investigate the behaviour of complex oxide systems at high temperature. It is also useful to apply a rational concept, based on the cation-sublattice, towards the understanding of phase relations and the development of design criteria for oxide coatings.

Acknowledgements

The authors gratefully acknowledge the financial support from the Spanish Government (projects CEN 2007-2014, MAT2010-18519 and SURFALUX SOL-00030930), DGA (Laser Applications Laboratory T87) and Fundación Domingo Martínez.

References

- [1] L. A. Martínez-Cruz, A. Ramos-Gallardo, A. Vegas, J. Solid State Chem. 110 (1994) 397-[398](#).
- [2] A. Ramos-Gallardo, A. Vegas, J. Solid State Chem. 128 (1997) 69-[72](#).
- [3] A. Vegas, M. Jansen, Acta Crystallogr., Sect. B: Struct. Sci. B58 (2002) 38-[51](#).
- [4] A. Vegas, V. García-Baonza, Acta Crystallogr., Sect. B: Struct. Sci. 63 (2007) 339-[345](#).
- [5] V. A. Blatov, Structure and Bonding 138 (2011) DOI: 10.1007/430_2010_34.
- [6] M. O'Keeffe, B. G. Hyde, Structure and Bonding 61 (1985) 77-[144](#).
- [7] Y. Waku, H. Ohtsubo, N. Nakagawa, Y. Kohtoku, J. Mater. Sci. 31 (1996) 4663-[4670](#).
- [8] Y. Waku, N. Nakagawa, T. Wakamoto, H. Ohtsubo, K. Shimizu & Y. Kohtoku, Nature 389 (1997) 49 - [52](#).
- [9] T. [Mah](#), T. [A. Parthasarathy](#), [L. E. Matson](#), Ceram. Eng. Sci. Proc. 11 (1990) 1617-[1627](#).
- [10] T.A. Parthasarathy, T. [Mah](#), L. E. Matson, J. Am. Ceram. Soc. 76 (1993) 29-[32](#).
- [11] J.Y. Pastor, J. Llorca, A. Salazar, P.B. Oliete, I. de Francisco, J.I. Peña, J. Am. Ceram. Soc. 88 (2005) 1488-[1495](#).
- [12] A. Larrea, G.F. de la Fuente, R.I. Merino, V.M. Orera, J. Eur. Ceram. Soc. 22 (2002) 191-[198](#).

Con formato: Inglés
(Estados Unidos)

Con formato: Español
(alfab. internacional)

- [13] M. Mora, C. López-Gascón, L. A. Angurel, G. F. de la Fuente, *Supercond. Sci. Technol.* 17 (2004) 1329-1334.
- [14] V. V. Lennikov, J. M. Pedra, J. J. Gómez, J. B. Carda, G. F. de la Fuente, *Solid State Sciences* 9 (2007) 404-[409](#).
- [15] C. Estepa and G. F. de la Fuente, P 200600560.
- [16] M. Jansen, *Angew. Chem. Int. Ed.* 41 (2002) [3746-3766](#).
- [17] H. Yasuda, I. Ohnaka, Y. Mizutani, Y. Waku, *Sci. Technol. Adv. Mater.* 2 (2001) 67-[71](#).
- [18] S. Lakiza, O. Fabrichnaya, Ch. Wang, M. Zinkevich, F. Aldinger, *J. Euro. Ceram. Soc.* 26 (2006) 233-[246](#).
- [19] K. A. Gschneidner, Jr., F. W. Calderwood, *Bull. Alloy Phase Diagrams* 9 (1988) 680.
- [20] [J. Zhang, H. Su, L. Liu, H. Fu, Mater. Sci. Forum 561-565 \(2007\) 999-1002.](#)
- [21] [H. Su, J. Zhang, S. Jiao, L. Liu, H. Fu, Adv. Mater. Res. 160-162 \(2011\) 773-776.](#)
- [22] Y. Mizutani, H. Yasuda, I. Ohnaka, Y. Waku, *Materials Trans.* 42 (2001) 238-244.
- [23] D. Errandonea, D. Santamaría-Pérez, A. Vegas, J. Nuss, M. Jansen, P. Rodríguez-Hernández, A. Muñoz, *Physical Review B: Condens. Matter* 77 (2008) 094113.
- [24] I.A. Bondar, L.N. Koroleva, E. T. Bezruk, *Inorg. Mater.* 20 (1984) 214.
- [25] [B. Mayer, H. Anton, E. Bott, M. Methfessel, J. Sticht, J. Harris, P.C. Schmidt, Intermetallics 11 \(2003\) 23-32.](#)

Con formato: Inglés
(Estados Unidos)

Con formato: Inglés
(Estados Unidos)

[26] [D.J. Thoma, J.H. Perepezco, D.H. Plantz, R.B. Schwarz, Mater. Sci. Eng. A179/A180 \(1994\) 176-180.](#)

Con formato: Inglés
(Estados Unidos)

[27] [N. L. Ross, R. Hazen, Phys. Chem. Minerals 17 \(1990\) 228.](#)

[28] [R.J. Angel, L.W. Finger, R.M. Hazen, M. Kanzaki, D.J. Weidner, R.C.](#)

[Liebermann, D.R. Veblen, Am. Mineral. 74 \(1989\) 509.](#)

Con formato: Español
(España - alfab.
tradicional)

Figure Captions

Figure 1. Laser Zone Melting apparatus used for this work. It includes a SLAB type CO₂ laser resonator, an optical beam steering system which focuses [the](#) laser beam onto a line at the coated substrate surface within a continuous furnace (not shown, see ref. 15). The substrate is moved at a constant rate in an orthogonal direction to the laser line focus.

Figure 2. XRD [diagram](#) of samples obtained by LZM using nominal compositions Y₁ (YAlO₃) (a) and Y₂ (Y₃Al₅O₁₂) (b): **+** - Y₃Al₅O₁₂ phase, **▼** - Al₂O₃ phase.

Figure 3. XRD [diagram](#) of samples obtained by LZM using nominal compositions Gd₁ (GdAlO₃) (a) and Gd₂ (Gd₃Al₅O₁₂) (b): **+** - GdAlO₃ phase, **▼** - Al₂O₃ phase.

Figure 4. Secondary electron micrograph of the interface between the [LZM](#) coating and the [Al₂O₃](#) substrate. (a) Sample Y₁ ([YAlO₃](#)), (b) Sample Y₂ ([Y₃Al₅O₁₂](#)), (c) Sample G₁ ([GdAlO₃](#)) and (d) Sample G₂ ([Gd₃Al₅O₁₂](#)).

Figure 5. Elemental microanalysis areas taken on sample Y₁ ([YAlO₃](#)) [across](#) the coating-substrate interface. Analyses were performed in the rest of samples in a similar fashion.

Figure 6. Secondary electron micrograph of the coating [corresponding to composition](#) [Y₁ \(YAlO₃\)](#). Faceted α-Al₂O₃ zones (a) Sample Y₁ ([YAlO₃](#)) grown at 1500 mm h⁻¹, (b) Sample Y₁ ([YAlO₃](#)) grown at 3000 mm h⁻¹.

Figure 7. Variation of the nanoindentation hardness [as a function of sample depth for](#) (a) Sample G₁ ([GdAlO₃](#)) grown at 1500mm h⁻¹, (b) Sample G₂ ([Gd₃Al₅O₁₂](#)) grown at 3000 mm h⁻¹.

Figure 8. Illustration of the crystallographic transformation between spinel (Fe₂SiO₄) and garnet (Fe₅Si₃O₁₂). [Left: illustration of the hypothetical Al₂LnO₄ spinel structure,](#)

Con formato: Español
(alfab. internacional)

exhibiting a truncated tetrahedron formed by 12 Al atoms centered around the L_n atom.

Center: insertion of two fictitious atoms in the upper and lower edges of the Al_{12} truncated tetrahedron. When one of these atoms is removed, the remaining atoms migrate towards the centre of the old edges, forming thus a new Al_{10} polyhedron. Right:

final Al_{10} polyhedron, existing within the $L_nAl_5O_{12}$ garnet.